

A note on stabilizing the Benjamin–Feir instability

By GUANGYU WU, YUMING LIU AND DICK K. P. YUE†

Department of Mechanical Engineering, Massachusetts Institute of Technology,
Cambridge, MA 02139, USA

(Received 23 August 2005 and in revised form 17 November 2005)

In a recent paper, Segur *et al.* (*J. Fluid Mech.* vol. 539, p. 229, 2005, hereafter referred to as \mathcal{S}) showed, based on a damped version of the nonlinear Schrödinger equation (NLS), that any amount of dissipation (of a certain type) stabilizes the Benjamin–Feir instability of a modulated Stokes wave train. Their theoretical predictions are confirmed by laboratory experiments for waves of small or moderate amplitude, but not for waves of large amplitude or with relatively large perturbations. \mathcal{S} left open questions regarding the validity of their theoretical results for these large-amplitude waves, and possibly the validity of the NLS assumptions of weak nonlinearity and narrow-bandedness. We investigate these issues using direct simulations of the primitive equations, incorporating constant and wavenumber-dependent dissipation models. For small or moderate amplitudes, our full simulations agree with the theory and experiments of \mathcal{S} . For large amplitudes, we find that it is primarily the form of the dissipation model, rather than the assumptions of NLS, that is responsible for the failure of \mathcal{S} 's theoretical predictions. Indeed, with an appropriate wavenumber-dependent dissipation model, both the full simulations and NLS obtain the correct evolution behaviour for large-amplitude waves. Finally, using direct and NLS simulations, we confirm the general conclusion of \mathcal{S} for stabilization of the Benjamin–Feir instability over long-time wave train evolution.

1. Introduction

It is well-known that unstable sideband disturbances will exponentially grow in the nonlinear evolution of a modulated wave train as a result of the Benjamin–Feir instability (Benjamin & Feir 1967). Recently, Segur *et al.* 2005, referred to herein as \mathcal{S} , used a damped version of the nonlinear Schrödinger equation (NLS):

$$\psi_t + \frac{\omega_0}{2k_0} \psi_x + i \frac{\omega_0}{8k_0^2} \psi_{xx} + i \frac{\omega_0 k_0^2}{2} |\psi|^2 \psi + \psi \delta = 0 \quad (1.1)$$

to show theoretically that the presence of dissipation diminishes the unstable region of disturbances in time so that all initial unstable disturbances become stable eventually, i.e. dissipation stabilizes the instability. In (1.1), $\psi(x, t)$ represents the complex amplitude of the envelop of the wave train, ω_0 and k_0 are respectively the frequency and wavenumber of the carrier wave, and $\delta (\geq 0)$ is a constant dissipation rate (e.g. Lo & Mei 1985). \mathcal{S} also conducted tank measurements which supported the theory for small to moderate carrier wave amplitudes and/or initial perturbations.

† Author to whom correspondence should be addressed. yue@mit.edu.

Although the theoretical result of \mathcal{S} is correct, and a similar finding was obtained by Mei & Hancock (2003) in the study of wave transmission over a random seabed, the conclusion of \mathcal{S} is somewhat surprising because it has been generally held that, while the presence of dissipation reduces the growth rate of unstable disturbances (Benjamin & Feir 1967; Lake & Yuen 1977) and changes the long-time evolution (Lo & Mei 1985), it does not affect the overall instability. Furthermore, for reasons \mathcal{S} discussed, their key conclusion had not been borne out by other measurements.

From the point of view of whether a Stokes wave train subject to (small) dissipation is indeed stable or not in the presence of sideband disturbances, \mathcal{S} leaves open a number of important questions: (a) \mathcal{S} is based on NLS which assumes narrow-band and weak nonlinearity. Does their result also hold for more general wave conditions (broad band and large amplitude) where the assumptions of NLS do not hold? (b) \mathcal{S} used a relatively simple dissipation model in (1.1). If a different dissipation model is required for the physical mechanism and a similar theoretical result might not be easy to obtain, would \mathcal{S} 's general conclusion still hold? (c) One major area of concern in \mathcal{S} is when the amplitude of the wave or the initial disturbance is large. In this case, the theory and measurements do not agree, and the question is whether (1.1) is valid for these waves and, more importantly, whether the conclusion of the Benjamin–Feir stability based on (1.1) indeed holds for these waves. (d) \mathcal{S} 's measurements were limited to relatively early evolution due to the length of their wave tank. The long-time evolution prediction of their theory was thus not verified (except for a special case they considered). Could the stabilizing effect they predicted be confirmed in long-time wave evolutions?

In this note, we address these issues using direct nonlinear wave simulations based on full Euler equation without resorting to model equations such as NLS.

2. Direct simulation model

We consider the problem of the nonlinear evolution of long-crested water waves in finite depth including the effects of dissipation and surface tension. In the context of potential flow, the field equation and boundary conditions (in Zakharov form) are (e.g. Dommermuth & Yue 1987)

$$\Phi_{xx} + \Phi_{zz} = 0 \quad \text{for } z \leq \eta(x, t), \quad (2.1)$$

$$\eta_t + \eta_x \Phi_x^S - (1 + \eta_x^2) \Phi_z = 0 \quad \text{at } z = \eta(x, t), \quad (2.2)$$

$$\Phi_t^S + g\eta + \frac{1}{2}(\Phi_x^S)^2 - \frac{1}{2}(1 + \eta_x^2) \Phi_z^2 - \mathcal{T} \eta_{xx} (1 + \eta_x^2)^{-3/2} + D_\phi = 0 \quad \text{at } z = \eta(x, t), \quad (2.3)$$

$$\Phi_z = 0 \quad \text{at } z = -h, \quad (2.4)$$

where $\eta(x, t)$ is the free-surface elevation, $\Phi(x, z, t)$ the velocity potential, $\Phi^S(x, t) \equiv \Phi(x, z = \eta, t)$ the velocity potential on the free surface, h the water depth, g the gravitational acceleration, and \mathcal{T} the surface tension. Here (2.2) and (2.3) are the nonlinear kinematic and dynamic free-surface boundary conditions, respectively, and D_ϕ is included in (2.3) as a quasi-potential approximation to account for the (viscous) dissipation effect (e.g. Ruvinsky, Feldstein & Freidman 1991).

For simplicity, a constant-dissipation model, i.e. $D_\phi \propto \Phi$, is often used in (2.3) (e.g. Jiang *et al.* 1996). A more physically realistic dissipation model accounting for viscosity effect obtains, upon balancing of normal stress on the free surface, that $D_\phi \propto \Phi_{zz}$ (e.g. Ruvinsky *et al.* 1991; Zhang & Vinals 1997). To elucidate the importance of the

dissipation modelling, we consider in this note both of the above models:

$$\text{Model I : } \quad D_\phi = \Phi^S \delta_1, \quad (2.5)$$

$$\text{Model II : } \quad D_\phi = \Phi_{zz} \delta_2, \quad (2.6)$$

where δ_1 and δ_2 are the dissipation coefficients to be determined by the practical environmental conditions. For a single (linear) regular wave with wavenumber k_0 , (2.5) becomes equivalent to (2.6) by setting $\delta_1 = k_0^2 \delta_2$. The dissipation rate in Model I (strictly for a linear wave train) is independent of the wavenumber k of the wave component, which is also the case in (1.1). For Model II, the dissipation rate is proportional to k^2 , consistent with classical theory (Lamb 1932; Longuet-Higgins 1997). A similar dissipation model to (2.6) in the context of (2.1)–(2.4) was used by Skandrani, Kharif & Poitevin (1996) to show that the presence of such a dissipation promotes the frequency downshift in the nonlinear evolution of a wave train. They did not, however, address the issue of stabilization of the Benjamin–Feir instability in that context.

We apply the high-order spectral method (HOS) (e.g. Dommermuth & Yue 1987) to directly solve the nonlinear wave evolution problem (2.1)–(2.4). HOS is a pseudo-spectral method based on the mode-coupling idea. The method follows the evolution of a large number, \mathcal{N} , of (broadband) wave modes and accounts for their nonlinear interactions up to an arbitrary order, \mathcal{M} , in the wave steepness. In particular, the method achieves exponential convergence with respect to \mathcal{N} and \mathcal{M} for moderately steep waves. The efficacy of HOS has been established in the study of the nonlinear wave–wave interaction mechanism (e.g. Dommermuth & Yue 1987) including the presence of atmospheric forcing (Dommermuth & Yue 1988), long–short waves (Zhang, Hong & Yue 1993), and finite depth and depth variations (Liu & Yue 1998).

3. Comparison of direct simulations with experiments

We perform direct comparisons between the HOS simulations and the experiments of \mathcal{S} to examine the validity of the NLS assumptions and investigate the effect of dissipation modelling on stabilizing the Benjamin–Feir instability. Special attention is paid to the case of large waves or disturbances for which the theoretical result and experiments of \mathcal{S} do not agree. Based on (1.1), \mathcal{S} showed that in the (time) evolution of a modulated Stokes wave train, the two integral quantities below (which are conserved in the absence of dissipation) must decay exponentially with time:

$$M(t) \equiv \frac{1}{L} \int_L |\psi(x, t)|^2 dx = M(0)e^{-2\delta t}, \quad P(t) \equiv \frac{i}{L} \int_L [\psi \psi_x^* - \psi^* \psi_x] dx = P(0)e^{-2\delta t} \quad (3.1)$$

where $*$ denotes the complex conjugate and L is the length of the periodic domain of the NLS. The theoretical results (3.1) are confirmed by their experiments for waves of small to moderate amplitude, but not when the wave amplitude is large. Specifically, the experiments show that, for large waves, P changes sign from positive to negative during the evolution, in contrast to (3.1).

\mathcal{S} considered two key wave experiments: one small amplitude and the other large amplitude. Table 1 gives the relevant parameters, where δ_e is the measured dissipation rate obtained by fitting the experimentally measured $M(x)$ with the exponential decay, $M(x) = M(0)e^{-2\delta_e x}$. (Note that, for the spatial evolution of the wave train in the tank, $M(x)$ here is the counterpart of the temporal evolution $M(t)$ in the NLS in (3.1)).

	$a_{\pm 1}/a_0$	$k_0 a_0$	δ_e
Small amplitude:	0.14	0.1	0.11 m ⁻¹
Large amplitude:	0.33	0.093	0.12 m ⁻¹

TABLE 1. Initial amplitude ratio of sidebands to carrier wave $a_{\pm 1}/a_0$, initial carrier wave steepness $k_0 a_0$, and measured dissipation rate δ_e of the two laboratory experiments in \mathcal{S} .

Both experiments have the same carrier wave frequency $\omega_0 = 20.923 \text{ s}^{-1}$, similar initial carrier wave steepness $k_0 a_0$ and dissipation rate δ_e , but different initial sideband amplitudes $a_{\pm 1}$. The frequencies of the sidebands are $\omega_{\pm n} = \omega_0 \pm n \Delta\omega$, $n = 1, 2, \dots$, with $\Delta\omega = 1.068 \text{ s}^{-1}$. The time history of the free-surface displacement is measured at 12 locations in the tank with the distance from the wavemaker (in cm) of $X_m = 78 + 50m$, $m = 1, \dots, 12$. The water depth is $h = 20 \text{ cm}$.

In the HOS simulations, the initial free-surface elevation and velocity potential are obtained from the experimental measurements at $x = X_1$ using linear theory:

$$\eta(x, 0) = \sum_i A_i \cos \theta_i \Big|_{t=0}, \quad \Phi^S(x, 0) = \sum_i \frac{A_i \omega_i}{k_i \tanh k_i h} \sin \theta_i \Big|_{t=0}, \quad (3.2)$$

where $\theta_i \equiv k_i x - \omega_i t + \alpha_i$, and A_i , α_i , and ω_i are the amplitude, phase, and frequency of the i th Fourier component of the wave displacement measured experimentally at $x = X_1$. Since the wave energy is concentrated in a small neighbourhood of ω_0 in the experiments, we use only the free wave components in the band $\omega_i \in [0.5\omega_0, 1.5\omega_0]$ for the initial conditions $\eta(x, 0)$ and $\Phi^S(x, 0)$. The wavenumber k_i is related to the corresponding frequency ω_i by the dispersion relation: $\omega_i^2 = (gk_i + \mathcal{T}k_i^3) \tanh k_i h$. The coefficients in the two dissipation models (2.5) and (2.6) are obtained by equating the respective linear spatial dissipation rates of the carrier wave to the measured δ_e :

$$\delta_1 = 2c_{g0}\delta_e, \quad \delta_2 = 2c_{g0}\delta_e/k_0^2, \quad (3.3)$$

where c_{g0} is the group velocity of the carrier wave.

The length of the HOS computational domain is $L = 100\lambda_0 (\equiv 200\pi/k_0)$. A periodic boundary condition in x is used with non-periodic components in $\eta(x, 0)$ and $\Phi^S(x, 0)$ tapered in small regions at the two ends of the domain. The other computational parameters are: $\mathcal{N} = 4096$, $\mathcal{M} = 4$, and time step $\Delta t = T_0/64 \equiv \pi/32\omega_0$. With these parameters, the maximum error (by comparing to simulations obtained with $\mathcal{N} = 8192$ and $\mathcal{M} = 5$) in the amplitudes of the carrier wave and sidebands after $O(100T_0)$ is less than 0.1%. As in standard HOS, energy accumulating at the top of the wavenumber range is removed by low-pass filtering. For these simulations, typically less than 0.01% of the total energy is lost per wave period of simulation due to filtering. Similar to the NLS, the temporal (t) evolution of the HOS wave field for the i th wave component is compared to the spatial (x) evolution of the wave train in the experiment by setting $t = x/c_{gi}$, where c_{gi} is the group velocity of i th component.

In figure 1, HOS results are compared to the experiments of \mathcal{S} for the amplitudes of the carrier wave (a_0) and upper and lower sidebands ($a_{\pm 1}$) as functions of distance from the wavemaker for the two cases in table 1. The experimental data for the large-amplitude case, which was not shown in \mathcal{S} , were provided by D. Henderson (one of the authors). As in \mathcal{S} , the wave amplitudes are compared in a frame with decaying effect, $e^{-\delta_e x}$, factored out (for clarity in comparison, the same factor is used in both Models I and II in plotting the results).

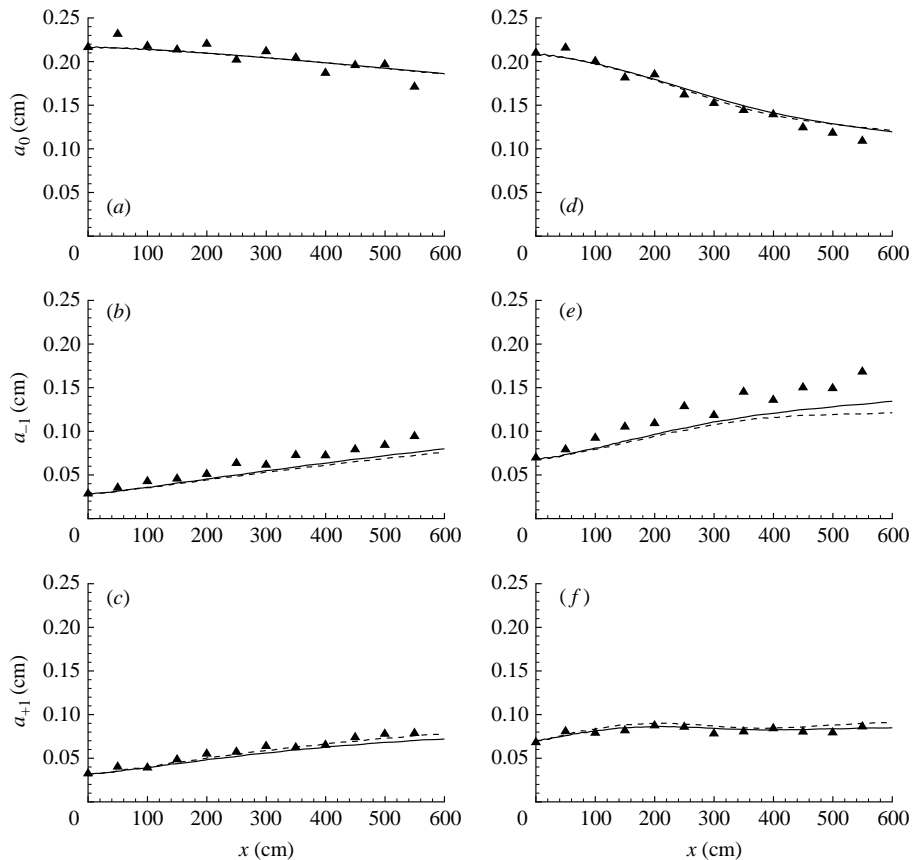


FIGURE 1. Comparisons of the HOS simulations (Model I: - - -; Model II: —) with the experiments of \mathcal{S} (\blacktriangle) for wave amplitudes in the decaying frame. (a, d) Carrier wave a_0 , (b, e) lower sideband a_{-1} and (c, f) upper sideband a_{+1} as functions of distance from the wavemaker for the evolution of small-amplitude (a–c) and large-amplitude (d–f) wave trains. ($x = 0$ is 128 cm from the wavemaker.)

The comparisons between direct simulations and experiments are satisfactory for both small and large wave trains using either dissipation model, although the simulations slightly underestimate the lower sideband. In both cases, the simulations with Model II provide a larger (smaller) prediction of lower (upper) sideband than those with Model I. In \mathcal{S} , the amplitudes of higher harmonic sidebands, $a_{\pm 2}$ and $a_{\pm 3}$, were also obtained. We have also made comparisons of these to the direct simulations. Overall, the comparisons are also satisfactory and very similar to those in figure 1, with the results using Model II again generally slightly over/under predicting the higher harmonic lower/upper sideband amplitudes than those with Model I.

In figure 2, we compare HOS simulations with the measurements of \mathcal{S} for the integral quantities $M(x)$ and $P(x)$. In HOS, M and P are computed using (3.1) with the complex amplitude of the wave envelope at time t given by $\psi(x) = \eta(x, t)\exp(-ik_0x)$, where $\eta(x, t)$ is obtained from the simulation. Here M and P are plotted in the original physical frame instead of the decaying frame since P is not conserved in the decaying frame. For M , HOS predictions using either dissipation model are satisfactory for both small and large wave amplitude. For P , the comparisons are more qualitative,

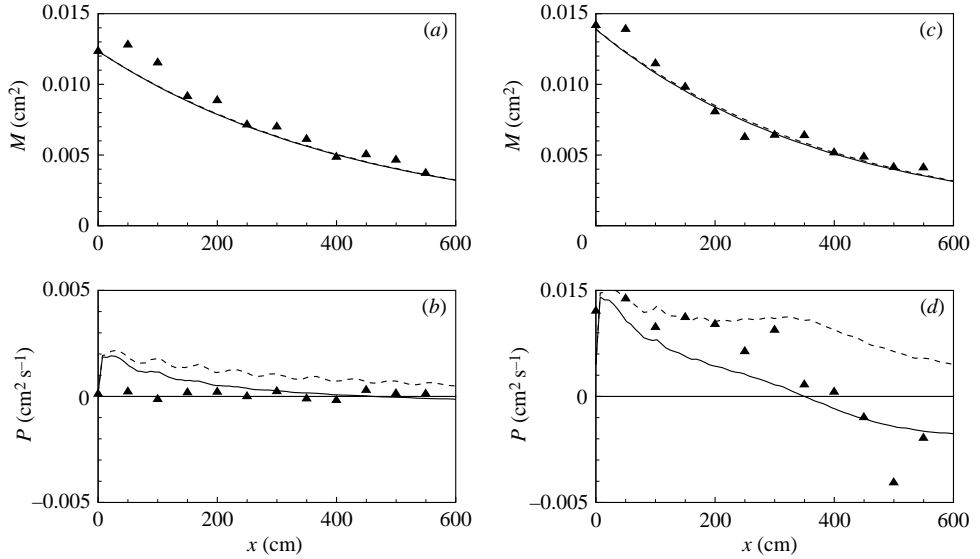


FIGURE 2. Comparisons of M and P as functions of distance from the wavemaker between HOS simulations (with Model I: - - -; and Model II: —) and the experiments of \mathcal{S} (▲) during nonlinear evolution of small-amplitude (a, b); and large-amplitude (c, d); wave trains.

with the Model II HOS predictions apparently better than those using Model I for the large-amplitude case. In particular, the change of sign of P in the experiment after some time for this case is predicted by HOS Model II. As reported by \mathcal{S} , the NLS predictions based on (1.1) fail for the large-amplitude case but are satisfactory for small amplitude (see figure 4 below). We note that the apparent discrepancy between HOS and the experiment at the initial time in figure 2(b) is due to the initial condition for HOS not including the bound waves that are present in the measurements at $x = X_1$.

The sign change of P in figure 2(d) and the prediction of it with dissipation Model II can be explained heuristically. For $\psi(x) = \sum_n a_n e^{in\Delta kx}$, we have $P = 2\Delta k \sum_n n |a_n|^2$, from its definition. Thus, higher-wavenumber upper sideband ($n > 0$, $k_n \equiv k_0 + n\Delta k > k_0$) components contribute positively to P , while lower sideband ($n < 0$, $k_n < k_0$) components contribute negatively. On the other hand, the dissipation rate in Model II is proportional to k^2 and hence disproportionately damps out the upper sideband components more rapidly relative to the lower sideband (cf. figures 1(e) and 1(f) for Model II relative to Model I predictions). For large-amplitude sidebands, this effect evidently becomes significant enough over time (distance) to cause P to become negative.

The small- and large-amplitude cases \mathcal{S} used are for similar carrier wave steepness but different perturbation amplitudes (table 1). To understand the effect of larger carrier wave steepness, we present results for two steeper carrier waves, $k_0 a_0 = 0.14$ and 0.18. The carrier wavenumber, normalized perturbation wavenumber and amplitude, and dissipation rate are otherwise the same as those for the small-amplitude case in table 1. Figure 3 shows the very long-time evolution of P for the steeper carrier wave cases using direct simulations with different dissipation models. The very long-time result for the small-wave case is also shown for comparison. With Model II, the value of P always decreases from positive to negative, reaches a minimum point, and then increases and approaches zero. The minimum value of P is smaller for larger carrier

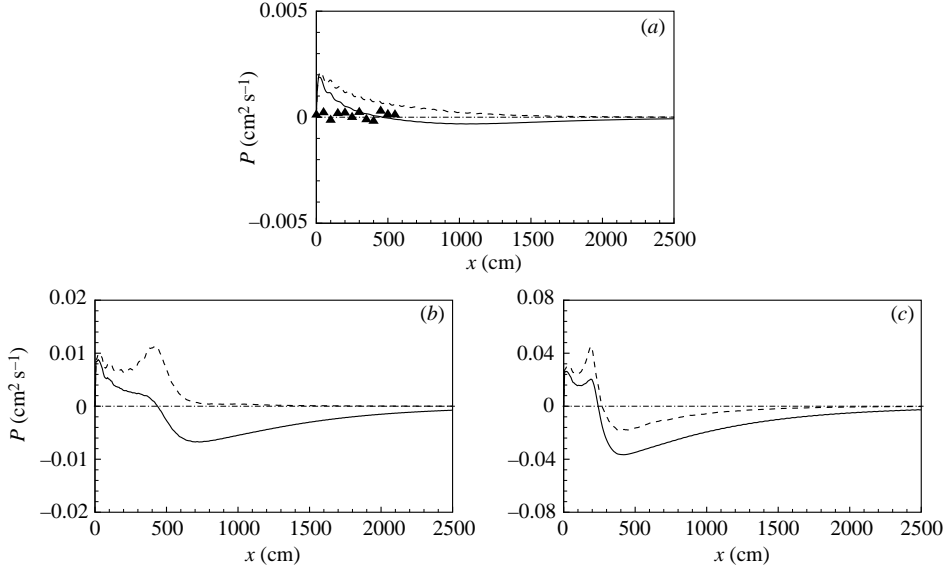


FIGURE 3. Effect of carrier wave steepness on the long-time evolution of P : (a) $k_0 a_0 = 0.10$ and $\Delta k/k_0 = 0.10$, (b) $k_0 a_0 = 0.14$ and $\Delta k/k_0 = 0.14$, and (c) $k_0 a_0 = 0.18$ and $\Delta k/k_0 = 0.18$; from measurements of \mathcal{S} (\blacktriangle) and HOS simulations with Model I (---) and Model II (—).

wave. With Model I, figure 3(c) shows that the asymmetric growth of sidebands induced by very strong nonlinear wave interactions can also change the sign of P . In figures 3(b) and 3(c), the initial peaks of P are due to the spread of energy to high frequency as a result of broadband wave interactions. In all cases, the absolute value of P eventually decays to zero as the total wave energy diminishes.

4. Modified form of the damped NLS

The results of §3 suggest that the difficulty in \mathcal{S} with the damped NLS (1.1) for the large-amplitude case, especially in predicting P , might be a result of the constant-dissipation model used (rather than the other assumptions in the NLS). To show that this is indeed the case, we make a simple heuristic modification to (1.1) by incorporating a wavenumber-dependent dissipation model comparable to (2.6):

$$\psi_t + \frac{\omega_0}{2k_0} \psi_x + i \frac{\omega_0}{8k_0^2} \psi_{xx} + i \frac{\omega_0 k_0^2}{2} |\psi|^2 \psi + (k_0^2 \psi - i 2k_0 \psi_x - \psi_{xx}) \delta_2 = 0. \quad (4.1)$$

The damping term associated with δ_2 above is constructed to obtain a dissipation rate proportional to k_n^2 for $\psi(x) = \sum_n a_n e^{in\Delta k x}$. Comparing (4.1) and (1.1), and letting $k_0^2 \delta_2 = \delta$, the additional terms introduced are $-i 2k_0 \psi_x \delta_2$ and $-\psi_{xx} \delta_2$. While the value of δ_2 in (4.1) can in principle again be related to that used in (2.6) by equating the net energy loss, the direct relationship between HOS with Model II and the variable-dissipation NLS (4.1) is in general non-trivial. From (4.1), it can be shown that:

$$\frac{dM}{dt} = -(2k_0^2 \delta_2) M - (2k_0 \delta_2) P - (2\delta_2) \frac{1}{L} \int_L |\psi_x|^2 dx \quad (4.2)$$

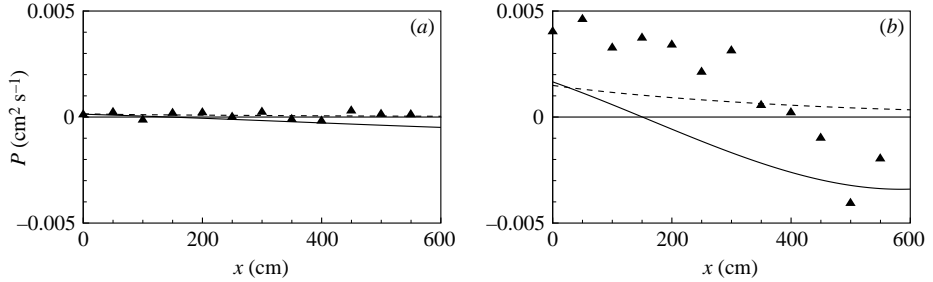


FIGURE 4. Comparisons of P as a function of distance from the wavemaker between theoretical predictions using damped NLS equations (1.1) (---) and (4.1) (—), and the experiments of \mathcal{S} (\blacktriangle) for (a) small- and (b) large-amplitude waves.

and

$$\frac{dP}{dt} = -(2k_0^2\delta_2)P - (2k_0\delta_2)\frac{1}{L}\int_L 4|\psi_x|^2 dx - (2\delta_2)\frac{i}{L}\int_L (\psi_x\psi_{xx}^* - \psi_x^*\psi_{xx}) dx, \quad (4.3)$$

where the second and third terms on the right-hand side of (4.2) and (4.3) are associated with the two additional dissipation terms in (4.1). Because of these terms, M and P do not decay purely exponentially with time. In particular, the second term on the right-hand side of (4.3) is negative definite and will always act to reduce the value of P with time (and possibly from positive to negative). Figure 4 compares the predictions of P using (1.1) versus (4.1) to the measurements of \mathcal{S} for small- and large-amplitude waves. The modified damped NLS (4.1) provides a qualitatively more realistic prediction of P for the large-amplitude wave case, in particular capturing the sign change from positive to negative. Quantitatively agreement however is still lacking.

5. Dissipation effect on long-time wave evolution

The key conclusion of \mathcal{S} , obtained based on (1.1), is that the presence of dissipation, no matter how small, will eventually stabilize the Benjamin–Feir instability. For the relatively limited evolution distance allowed by their experimental tank, this is confirmed (for the small-amplitude wave case). As a final check, we obtain long-time evolution predictions using direct HOS simulations (with Model II dissipation) as well as the modified damped NLS equation (4.1) for both small and large wave amplitudes.

Figure 5 plots the long-time evolution of the amplitudes of the carrier wave and the first sideband components (in the decaying frame) up to $x = 2500 \text{ cm} \sim 175\lambda_0$. Since the dissipation rate is now wavenumber-dependent, it is important that the decaying effect is factored out based on the actual dissipation rate of each wave component, i.e. $\exp(-\delta_e(k_i^2/k_0^2)x)$, $i = 0, \pm 1$. From the figure, it is clear that these wave components all eventually reach stable states. This confirms the general conclusion of \mathcal{S} , based originally on a constant-dissipation NLS model, that the presence of dissipation eventually stabilizes the Benjamin–Feir instability.

Figure 5 also shows a distinct frequency downshift for the large-amplitude case (see e.g. Skandrani *et al.* 1996). In fact the lower sideband amplitude a_{-1} eventually becomes greater than that of the carrier wave a_0 (in the decaying frame). In the present context, the frequency downshift depends not only on the parameters of the wave train but also on the dissipation rate, the latter diminishing the unstable

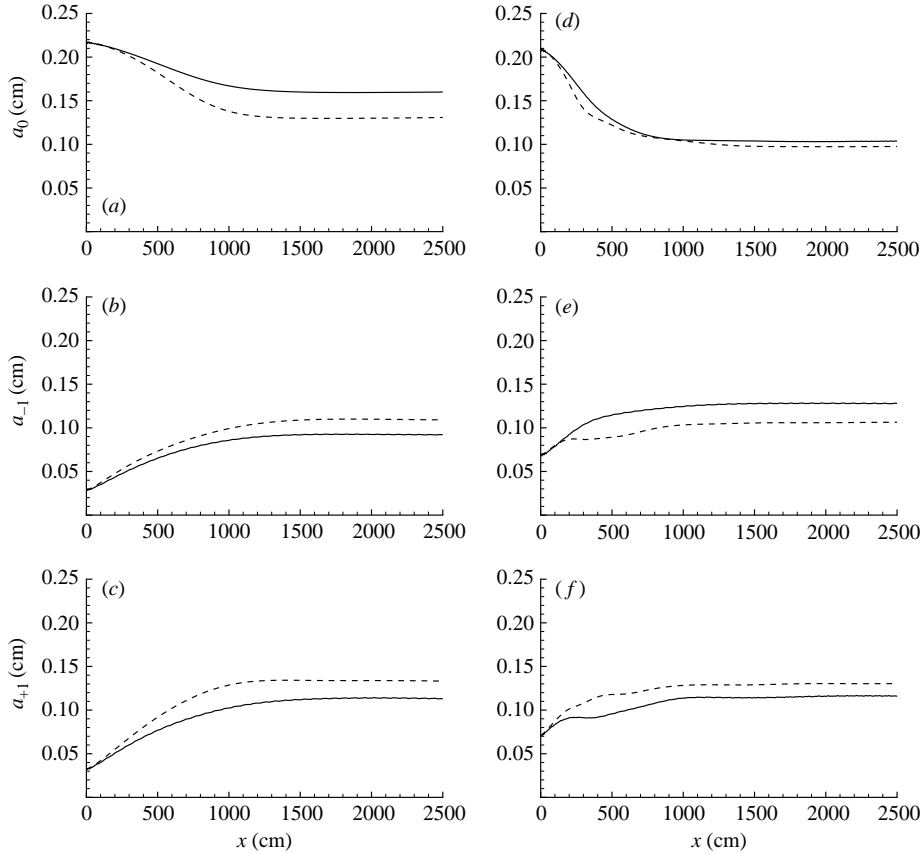


FIGURE 5. Long-time evolution of the amplitudes in decaying frame of (a, d) carrier wave a_0 , (b, e) lower sideband a_{-1} and (c, f) upper sideband a_{+1} , as functions of distance from the wavemaker during nonlinear evolution of small- (a–c) and large- (d–f) amplitude wave trains; obtained using direct HOS simulations with Model II dissipation (2.6) (—) and the modified damped NLS (4.1) (---).

region and changing the growth rate in time. Indeed, the magnitudes of the frequency downshift in the cases shown in figure 3(b, c) are much greater than would be obtained with the most unstable sideband disturbance for these wave trains given by classical inviscid stability theory.

6. Conclusions

We use direct simulations to address the question, raised in \mathcal{S} , of the stability and evolution of a sideband modulated Stokes wave train in the presence of dissipation. Our direct simulations, using HOS (with different dissipation models), agree with the theoretical and experimental predictions of \mathcal{S} for small- or moderate-amplitude waves. For large wave amplitudes, for which the theory and measurements of \mathcal{S} disagree, we find that the discrepancy is primarily due to the form of the dissipation term used in \mathcal{S} . This we confirm by showing that the NLS model equation using a new wavenumber-dependent dissipation model obtains reasonably satisfactory agreement with experiments for small and large wave amplitudes. Finally, we confirm by both

HOS and NLS simulations the theoretical conclusion of \mathcal{S} about long-time stabilizing of the Benjamin–Feir instability in the presence of dissipation.

We gratefully acknowledge stimulating discussions with Professors H. Segur and D. Henderson who also kindly provided us with the raw data of the experiments in \mathcal{S} . This research is supported financially by grants from the Office of Naval Research.

REFERENCES

- BENJAMIN, T. B. & FEIR, J. E. 1967 The disintegration of wave trains in deep water. Part 1. Theory. *J. Fluid Mech.* **27**, 417–430.
- DOMMERMUTH, D. G. & YUE, D. K. P. 1987 A high-order spectral method for the study of nonlinear gravity waves. *J. Fluid Mech.* **184**, 267–288.
- DOMMERMUTH, D. G. & YUE, D. K. P. 1988 The nonlinear three-dimensional waves generated by a moving surface disturbance. In *Proc. 17th Symp. on Naval Hydro., The Hague, Netherlands*. Washington DC: National Academy Press.
- JIANG, L., TING, C.-L., PERLIN, M. & SCHULTZ, W. W. 1996 Moderate and steep Farady waves: instabilities, modulation and temporal asymmetries. *J. Fluid Mech.* **329**, 275–307.
- LAKE, B. M. & YUEN, H. C. 1977 A note on some water-wave experiments and the comparison of data with theory. *J. Fluid Mech.* **83**, 75–81.
- LAMB, H. 1932 *Hydrodynamics*, 6th Edn. Cambridge University Press.
- LIU, Y. & YUE, D. K. P. 1998 On generalized bragg scattering of surface waves by bottom ripples. *J. Fluid Mech.* **356**, 297–326.
- LO, E. & MEI, C. C. 1985 numerical study of water-wave modulations based on a higher-order nonlinear schrodinger equation. *J. Fluid Mech.* **150**, 395–416.
- LONGUET-HIGGINS, M. S. 1997 Viscous dissipation in steep capillary-gravity waves. *J. Fluid Mech.* **344**, 271–289.
- MEI, C. C. & HANCOCK, M. J. 2003 Weakly nonlinear surface waves over a random seabed. *J. Fluid Mech.* **475**, 247–268.
- RUVINSKY, K. D., FELDSTEIN, F. I. & FREIDMAN, G. I. 1991 Numerical simulations of the quasi-stationary stage of ripple excitation by steep-capillary waves. *J. Fluid Mech.* **230**, 339–353.
- SEGUR, H., HENDERSON, D., CARTER, J., HAMMACK, J., LI, C., PHEIFF, D., & SOCHA, K. 2005 Stabilizing the Benjamin–Feir instability. *J. Fluid Mech.* **539**, 229–271 (referred to herein as \mathcal{S}).
- SKANDRANI, C., KHARIF, C. & POITEVIN, J. 1996 Nonlinear evolution of water surface waves: the frequency down-shift phenomenon. *Contemp. Math.* **200**, 157–171.
- ZHANG, J., HONG, K. & YUE, D. K. P. 1993 Effects of wavelength ratio on wave-mode modeling. *J. Fluid Mech.* **248**, 107–127.
- ZHANG, W. & VINALS, J. 1997 Pattern formation in weakly damped parametric surface waves. *J. Fluid Mech.* **336**, 301–330.